PAPER • OPEN ACCESS

Probing the role of CNTs in Pt nanoparticle/CNT/graphene nanohybrids H₂ sensors

To cite this article: Mohammed Alamri et al 2022 Nano Ex. 3 035004

View the article online for updates and enhancements.

You may also like

- Extreme elastic deformable ceramics on the nanoscale: Cr_xB_yO_z nanowire as an example G Csiszár, R Lawitzki and O Csiszár
- Superacid Treatment on Transition Metal Dichalcogenides Daisuke Kiriya and Der-Hsien Lien
- lonic gating in metallic superconductors: A brief review Erik Piatti





OPEN ACCESS

RECEIVED

3 April 2022

REVISED

27 May 2022

ACCEPTED FOR PUBLICATION

24 July 2022

PUBLISHED

18 August 2022

Original content from this work may be used under the terms of the Creative Commons Attribution 4.0 licence

Any further distribution of this work must maintain attribution to the author(s) and the title of the work, journal citation and DOL



PAPER

Probing the role of CNTs in Pt nanoparticle/CNT/graphene nanohybrids H₂ sensors

Mohammed Alamri^{1,2,5,*}, Bo Liu^{1,5,*}, Cindy L Berrie³, Michael Walsh⁴ and Judy Z Wu^{1,*}

- Department of Physics and Astronomy, The University of Kansas, Lawrence, Kansas 66045, United States of America
- ² Department of Physics, University of Umm Al-Qura, PO Box 56335, Makkah 21955, Kingdom of Saudi Arabia
- ³ Department of Chemistry, The University of Kansas, Lawrence, Kansas 66045, United States of America
- Department of Energy's National Security Campus, Kansas City, Missouri 64147, United States of America
- Contributing equally
- * Authors to whom any correspondence should be addressed.

E-mail: moomri@uqu.edu.sa, liubo@ku.edu and jwu@ku.edu

Keywords: atomic layer deposition, carbon nanotube, graphene, UV irradiation, gas sensor

Supplementary material for this article is available online

Abstract

In the carbon nanotubes film/graphene heterostructure decorated with catalytic Pt nanoparticles using atomic layer deposition (Pt-NPs/CNTs/Gr) H₂ sensors, the CNT film determines the effective sensing area and the signal transport to Gr channel. The former requires a large CNT aspect ratio for a higher sensing area while the latter demands high electric conductivity for efficient charge transport. Considering the CNT's aspect ratio decreases, while its conductivity increases (*i.e.*, bandgap decreases), with the CNT diameter, it is important to understand how quantitatively these effects impact the performance of the Pt-NPs/CNTs/Gr nanohybrids sensors. Motivated by this, this work presents a systematic study of the Pt-NPs/CNTs/Gr H₂ sensor performance with the CNT films made from different constituent CNTs of diameters ranging from 1 nm for single-wall CNTs, to 2 nm for double-wall CNTs, and to 10–30 nm for multi-wall CNTs (MWCNTs). By measuring the morphology and electric conductivity of SWCNT, DWCNT and MWCNT films, this work aims to reveal the quantitative correlation between the sensor performance and relevant CNT properties. Interestingly, the best performance is obtained on Pt-NPs/MWCNTs/Gr H₂ sensors, which can be attributed to the compromise of the effective sensing area and electric conductivity on MWCNT films and illustrates the importance of optimizing sensor design.

1. Introduction

The utilization of carbon nanotubes (CNTs) as the sensing materials for detection of various gas molecules has been explored for over a decade [1, 2]. Liquid sensors based on CNTs such as alcoholic sensor have also been reported [3, 4]. CNT films or networks can provide a large effective surface area for adsorption/desorption of gas molecules, and the follow-up electron transfer driven by the interactions between gas molecules and π electrons of CNT [5]. This leads to a charge doping effect on CNTs and hence a change in the resistance of the CNT film, which is measured as the sensor's response to gas molecules. However the weak physisorption of most gas molecules on CNTs and the associated poor sensing performance for gas sensors based on pristine CNTs [6, 7] have prompted introduction of nanostructured catalytic metals such as gold (Au), silver (Ag), platinum (Pt), and palladium (Pd) on CNTs. The decoration with catalytic Pt metal nanostructures was especially suitable for enhancing H₂ sensing by providing much stronger chemisorption of H₂ molecules and the follow-up dissociation of H-H bond [8], lowering the work function of Pt and consequently resulting in charge transfer from hydrogen to CNT [9]. While improved performance was reported on CNT-based hydrogen sensors with Pt catalyst [9–11] further enhancement of sensitivity through optimization of the sensor design is important.

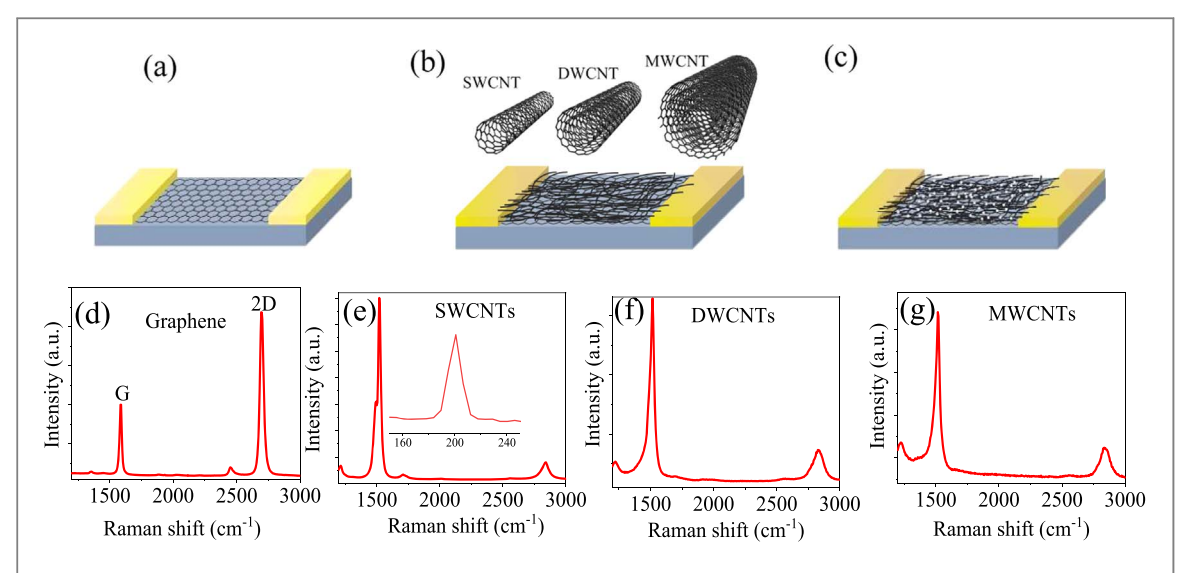
In a recent work [12], we have developed a 3D electrode architecture consisting of single-wall CNTs on graphene (SWCNT/Gr). The implementation of Gr of high charge mobility at room temperature [13, 14] has been found to effectively improve charge (signal) transfer by directing the charges from SWCNTs to electrodes through Gr, instead of through multiple CNT-CNT junctions to electrodes, which present hurdles to charge transfer in CNT only sensors. In addition, Gr is a semimetal and forms an Ohmic contact with common electrodes such as Au or Pd. [15–17]. Therefore, H₂ sensors consisting of a CNT film/graphene heterostructure 3D electrode decorated with catalytic Pt nanoparticles using atomic layer deposition (Pt-NPs/CNTs/Gr) combine the advantages of large effective sensing surface area of CNT films, the catalytic benefit of the conformally coated Pt-NPs, and high mobility signal transport through CNT/Gr 3D electrode. On the Pt-NP/ SWCNT/Gr H₂ sensors, enhanced H₂ sensitivity by more than 50% of magnitude has been observed as compared to their counterparts without Gr [12]. This result has revealed the critical importance of engineering the signal transfer on the 3D CNT/Gr electrodes while raises a question on whether SWCNT films are optimal for charge transfer. In fact, SWCNTs were chosen primarily because SWCNTs have the largest possible effective sensing area due to the highest aspect ratio (length versus diameter) among all CNTs with comparable lengths. However, SWCNTs tend to form bundles of an average diameter of ~ 10 nm, which considerably reduces the effective surface area of the SWCNT films [12]. In addition, most as-made SWCNTs using chemical vapor deposition are unpurified with about 2/3 semiconductive and 1/3 metallic SWCNTs. The inter-SWCNT junctions between the two kinds of SWCNTs are Schottky junctions and can hinder the charge transport [18] in SWCNT-based H₂ sensors. This means that SWCNTs may suffer limitations in reaching the optimal sensing surface area expected and poor charge transfer in the ideal case, both are critical parameters for highperformance H₂ sensors. Considering the bandgap of CNTs decreases inversely with the diameter of the CNTs [19, 20], higher conductivity is anticipated in CNTs with larger diameters including double-wall CNTs (DWCNTs) and multi-wall CNTs (MWCNTs). In addition, the issue of bundling would become less serious with decreasing aspect ratios as the CNT diameter increases. Considering both high effective sensing surface area and high conductivity are required for high-performance of the Pt-NPs/CNT/Gr nanohybrid H₂ sensors, a quantitative assessment of the effects of the CNT diameter and electrical conductivity on the sensor performance is important to obtaining optimal sensor design. Motivated by this, the objective of this work is to carry out a systematic investigation of the Pt-NPs/CNT/Gr nanohybrid H₂ sensor performance in correlation with the CNT morphology and electric conductance when the constituent CNT diameter in CNT films is increased from \sim 1 nm for SWCNTs, to \sim 2 nm for DWCNTs, and to \sim 10 nm-30 nm in MWCNTs. Interestingly, H₂ sensitivity has been found to be sensitively affected by the CNT selection and the highest H2 sensitivity has been achieved on Pt-NPs/MWCNT/Gr nanohybrid H_2 sensors in which the MWCNTs have ~10 nm in diameter.

2. Materials and methods

The Pt-NPs/CNT/Gr device fabrication involves four major steps of metal electrode deposition, graphene transfer, CNT film transfer and Pt-NP coating. In the first step, evaporation of Au electrodes was made on SiO_2/Si substrates. The dimensions of the Au electrodes are 4 mm (length) \times 2 mm (width) with a distance of 0.3 mm (regarded as device channel length) between neighboring Au bars. In the second step, a single-layer graphene strip was transferred onto the SiO_2/Si substrates with pre-fabricated Au electrodes (figure 1(a)). The graphene was synthesized using chemical vapor deposition (CVD) on commercial copper foils (Sigma-Aldrich) at ~ 1000 °C. The details of graphene growth and transfer were reported in previous works [21, 22]. In the third step, the CNT film was transferred on top of graphene to form the 3D CNT/Gr nanohybrid (figure 1(b)). The SWCNT, DWCNT and two kinds of MWCNT films studied in this work were prepared using a vacuum filtration method from dispersed CNT suspension solutions [23, 24]. This thicknesses of the CNT films were controlled by the filtration time or the total amount of CNTs based on the pre-calibrated rates for filtration from the corresponding CNT suspension solutions as we reported previously [12, 25]. Commercial (CheapTubes, Inc) SWCNTs (1-2 nm in diameter), DWCNTs (2-3 nm in diameter), smaller MWCNTs (10 nm) with CNT diameter of 10 nm, and larger MWCNTs (10-30 nm) due to the broader range of the CNT diameter were used to make CNT films of \sim 500 nm in thickness. The CNT lengths are in the range of 5–10 μ m. In the fourth step, the Pt-NPs, shown as grey spheres, were decorated conformally on the CNT/Gr electrodes using atomic layer deposition (ALD) by using alternating exposures to MeCpPtMe3 (Sigma-Aldrich) and oxygen pulses at 310 °C [12] (figure 1(c)). It should be noted that the Pt-NPs was found to nucleate on CNTs at low ALD pulse numbers and merge into a continuous Pt film with much reduced catalytic effect [12]. In this work, 20 ALD cycles (20 c) was selected in ALD Pt for Pt-NPs with an optimal catalytic effect in H₂ sensing.

Scanning electron microscopy (SEM) images and Energy-dispersive x-ray spectroscopy (EDS) spectra of the CNT/Gr nanohybrid samples with different cycle numbers of ALD-Pt coating were taken on Hitachi SU8230 Ultra-high Resolution Scanning Electron Microscope to extract the information of sample morphology and Pt

M Alamri et al



 $\begin{tabular}{l} Figure 1. (a) — (c) Schematic illustration of the Pt-NPs/CNTs/graphene H_2 gas sensor fabrication process: (a) Gr transferred on Si substrate with two pre-fabricated Au electrodes. (b) CNT films transferred on top of Gr. The CNT diameters are $1-2$ nm for SWCNTs, $2-3$ nm for DWCNTs, 10 or 30 nm for MWCNTs. (c) ALD coated $Pt-NPs$ (grey spheres) on CNT/Gr. Raman spectra of (d) Gr, (e) $SWCNTs, (f) DWCNTs, and (g) $MWCNTs$ films. } \end{tabular}$

element distribution. A WiTec Alpha300 confocal micro-Raman system equipped with a piezoelectric sample stage was used to collect Raman spectra and maps of graphene and CNTs on the CNT/Gr devices. Typically, a 488 nm laser was used as excitation light source in Raman spectroscopy and imaging. A Digital Instruments Multimode AFM system with a Nanoscope IIIa controller using standard silicon nitride cantilevers (NanoAndMore USA, $k=0.06,0.27~N~m^{-1}$) was used in contact mode with scan rates from 1–3 Hz to collect atomic force microscopy (AFM) images on the sample. For consistency, AFM images were collected from at least 3 different locations on each sample and the CNT dimensions were measured by averaging cross-sectional measurements of at least 20 nanotubes. The ultraviolet (UV) light (360 nm–400 nm) was used to activate the surface of CNT/graphene. The photoresponse of UV-irradiated sensor was measured to investigate the effect of UV on the performance of our sensor. The use of UV was to desorb air molecules from the CNT/graphene surface which allow more room for H_2 gas adsorption.

The H_2 response and sensitivity were characterized at room temperature in a vacuum chamber (volume ~500 cm³) under a mixed H_2/N_2 gas flow. The ALD-Pt-NPs/CNT/Gr sensors were mounted on a sample stage inside the chamber with a multi-pin electric feedthrough for the electric connection of the sample to external electronics. Before the measurement, the chamber was purged with a N_2 flow for about an hour to remove residual gas molecules. The concentration of H_2 was controlled by controlling the flow ratio of H_2 and N_2 gases using an MKS four-channel flowrate controller (MKS 946). In this work, the concentration of H_2 was varied in the range of 1% to 20% via changing the volume ratio of H_2 to N_2 buffer gases for the device sensitivity characterization. Current-time (I-t) curves were recorded on the Pt-NPs/CNT/Gr sensors at a constant bias voltage (V) using a CH Instruments CHI660D electrochemical workstation in response to the H_2 flow on and off in the vacuum chamber. The I-t curves were later converted to resistance-time (R-t) curves using Ohm's law R = VII where V was set 0.1 V in this work for the responsivity calculation. Resistance as function of temperature (R-t) curves were taken CNT films using a Keithley 224 current source (providing the bias currents) and a Keithley 2182 dc voltmeter (to record the voltage generated across the sample). Each device was exposed to H_2 gas for 1320 s (H_2 ON), followed with being in H_2 atmosphere for recover. The response of the device can return to its original state after a short exposure to air at room temperature (R-t).

3. Results and discussions

The architecture and fabrication procedure (details in Experimental) of Pt-NPs/CNT/Gr nanohybrid are schematically shown in figure 1. In this work three different types of CNTs - SWCNT, DWCNT and MWCNT - were compared. Gr is a semimetal and forms an Ohmic contact with Au electrodes as demonstrated in the linear I-V characteristic (figure S1 (available online at stacks.iop.org/NANOX/3/035004/mmedia)). The Raman spectra of Gr and the three different types of CNTs are shown in figure 1(d)–(g) respectively. The Raman spectrum of Gr exhibits the typical G peak at ~1604.9 cm⁻¹ and 2D peak at ~2692.5 cm⁻¹. The G and 2D peaks are related to the doubly degenerate zone center E_g^2 mode at the Brillouin zone center and the second order of

M Alamri et al

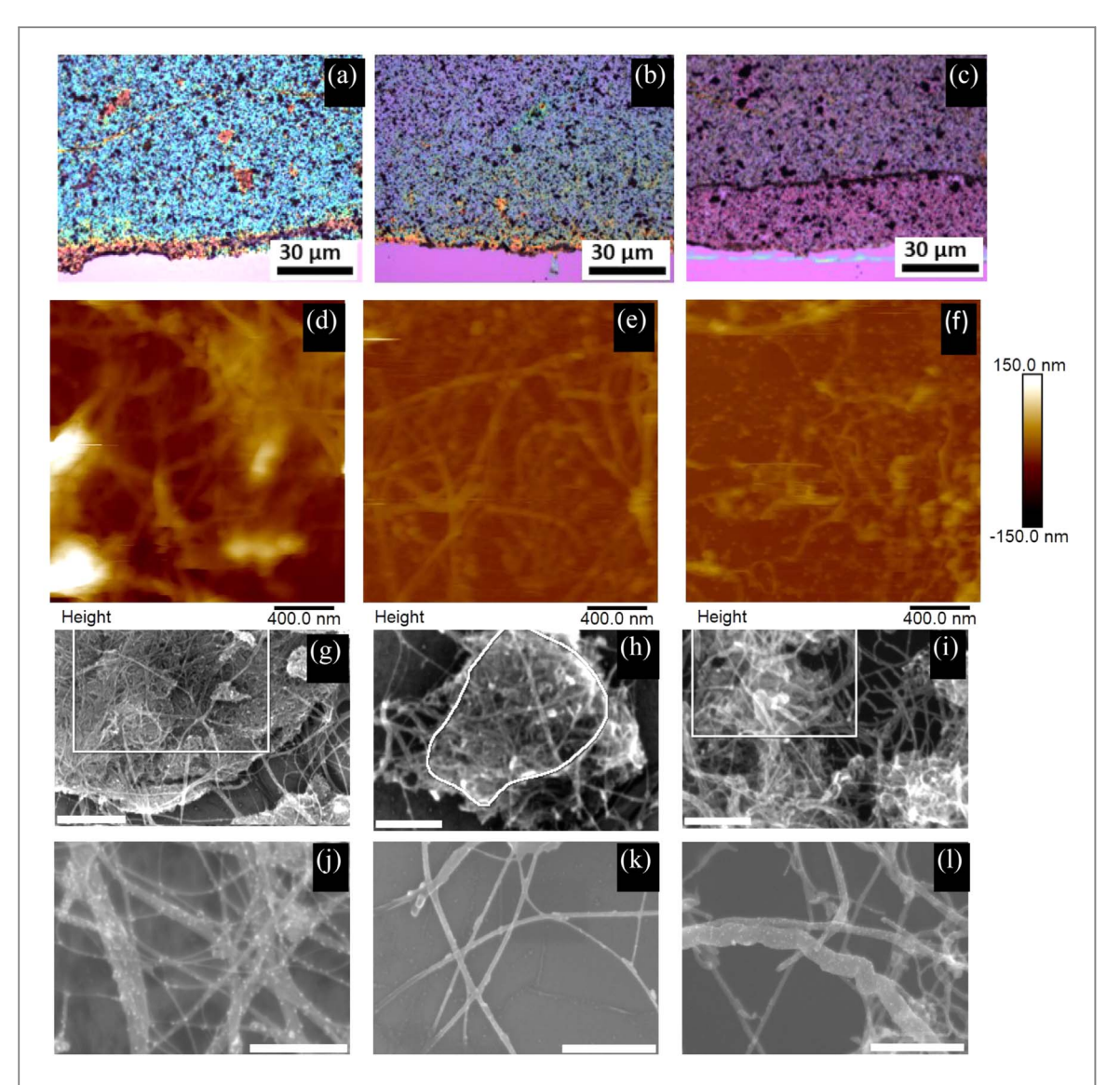


Figure 2. Optical, AFM, and SEM images of: (a), (d), (g), (j)) Pt-NPs/SWCNT/Gr, (b), (e), (h), (k) DWCNT/Gr, and (c), (f), (i), (l) MWCNT (10 nm)/Gr samples. Ruler bars for figures 2(g)—(i) and (j)—(l) are 250 nm and 200 nm, respectively.

zone-boundary phonons, respectively [26]. The absence of the D peak at ~1352.5 cm⁻¹ confirms that the Gr is the high quality with negligible defects. In addition, the high intensity ratio of the 2D peak to G peak of 2.3 indicates that the Gr is single-layer. In the Raman spectrum for SWCNT (figure 1(e)), the G peak splits into two peaks (G⁻ and G⁺ peaks) at 1496 cm⁻¹ and 1521 cm⁻¹ respectively in SWCNTs due to the curvature of the graphene sheet in the SWCNTs [27, 28]. Another distinctive peak is located at ~2833 cm⁻¹ corresponding to the 2D-band for SWCNTs [8]. The D peak at 1215 cm⁻¹ associated with the presence of in-plane defects on SWCNTs, possibly the growth defects that occurred during CVD synthesis of SWCNTs, is visible with low intensity, suggesting the defects are minor [29]. A single peak at 192.4 cm⁻¹ (the inset of figure 1(e)) is attributed to the radial breathing mode (RBM) of the SWCNTs [30, 31]. Due to a large diameter of the MWCNTs and DWCNTs, the characteristic RBM peak associated to smaller CNTs becomes too weak to be seen [32]. Therefore, the Raman spectra for DWCNT (figure 1(f)) and MWCNT (figure 1(g)) films look similar. In both cases, two distinct peaks at 1521 cm⁻¹ (G peak) and 2838 cm⁻¹ (2D peak) are clearly visible as anticipated from the high crystallinity of the DWCNTs and MWCNTs in addition to the D peak at 1215 cm⁻¹. Again, the low intensity of the D peak suggests the defects in DWCNTs and MWCNTs are insignificant.

The optical microscope images of the SWCNT, DWCNT and MWCNT (10 nm) films are displayed in figures 2(a)–(c), showing homogeneity over relatively large area of the film. The optical images and the Raman maps of a representative MWCNT (10 nm)/Gr device before and after the CNT was transferred on Gr are shown in figure S2 from which a uniform Gr channel and the CNT film on top can be seen clearly. The AFM images shown in figures 2(d)–(f) reveal porous structures of the CNT films at a microscopic scale, which is desired for gas sensors to provide a large sensing surface area, for the SWCNT, DWCNT, MWCNT (10 nm in diameter). Specifically, the diameter of the tube-like features, determined from the AFM cross-sectional heights, are

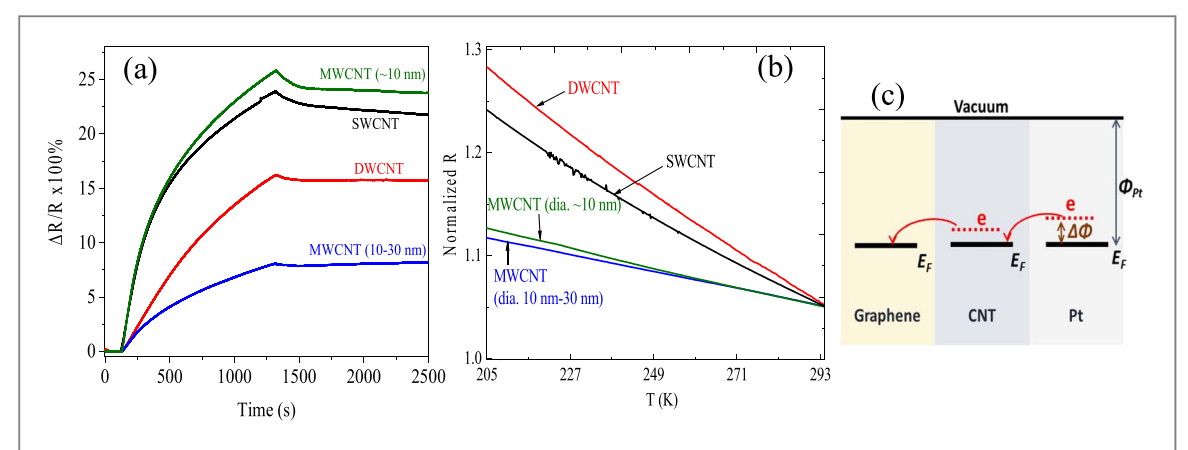


Figure 3. (a) Responsivity of H_2 gas sensor with 10% of H_2 of Pt-NPs/CNT/graphene sensors using four different kinds of CNTs: SWCNTs (black), DWCNTs (red), MWCNTs (10 nm, green), and MWCNTs (10–30 nm, blue). (b) R-T curves of the SWCNTs, DWCNTs, and MWCNTs (10 nm) and MWCNTs (10 nm–30 nm) films. (c) Schematic illustration of the sensing mechanism.

 10 ± 7 nm, 15 ± 6 nm and 16 ± 7 nm respectively for the SWCNT, DWCNT and MWCNT shown in figures 2(d)–(f), respectively. In the two former cases, the diameters measured for the tube-like features in these images are larger considerably than the anticipated for the constituent SWCNT and DWCNT, indicating the CNT bundling in these two cases. In the MWCNT, the issue of bundling is much less of concern since the AFM measured diameter is close to the anticipated one for the MWCNTs of 10 nm in diameter. Figures 2(g)–(l) display the SEM images of the SWCNT/Gr, DWCNT/Gr, MWCNT (10 nm)/Gr nanohybrids decorated with ALD Pt-NPs. Figures 2(g)–(i) are the zoom-out SEM images of the same samples, illustrating the network structure of CNT films. As seen in figure 2(g), SWCNTs tend to assemble into bundles with the diameter considerably larger than 1–2 nm. However, the amount of CNT bundling is expected to be less in the samples of DWCNT and MWCNT films because of their smaller aspect ratios and hence better dispersibility in water than their SWCNT counterpart's. Less bundling represents more effective sensor surface area, which is important to the gas sensor performance. In all three samples, Pt-NPs are uniformly and sparsely distributed surrounding the walls of CNTs. The diameter of Pt-NPs is a few nanometers and the mass fraction (wt%) is in the range of 1%-4% from EDS (figure S3), which is consistent with our previous result [12].

The responsivity (or sensitivity) of the Pt-NPs/CNTs/Gr devices to H₂ gas is defined as

Responsivity (
$$\Delta R/R_0\%$$
) = $\frac{R-R_0}{R_0}$ x100

Where R_0 and R are the resistances of the sensor before and after the exposure to H_2 , respectively [33]. Figure 3(a) compares the dynamic response to 10% of H_2 gas of the Pt-NPs/SWCNTs/Gr (black), Pt-NPs/DWCNTs/Gr (red), Pt-NPs/MWCNTs (10 nm)/Gr (green), and Pt-NPs/MWCNTs (10–30 nm)/Gr (blue) devices. The Pt-NPs/MWCNTs (10 nm)/graphene device exhibits the best sensitivity of 26% among the four samples. The Pt-NPs/SWCNTs/Gr device shows a slightly lower sensitivity of 24%. This could be attributed to the bundling of SWCNTs to form a larger diameter similar to that of MWCNTs (10 nm), resulting in a comparable sensor surface area to that of the MWCNTs (10 nm). The Pt-NPs/DWCNTs/Gr device shows a considerably lower H_2 responsivity of 16% while the lowest responsivity <10% was measured on the Pt-NPs/MWCNTs (10–30 nm)/Gr device.

In order to understand the difference in the H_2 sensitivity, responsivity measured on the four kinds of Pt-NPs/CNTs/Gr devices, figure 3(b) compares the normalized R-T curves of different types of CNT films. Although all four CNT films exhibit semiconductive behavior with resistance increasing with decreasing temperatures, a quantitative difference in the temperature dependence exists. The two MWCNT samples have the lowest temperature dependence due to the metallic behavior of MWCNTs. However, the DWCNT sample has a larger temperature dependence than its SWCNT counterpart does though its E_g is expected to be considerably smaller than the latter's. This may be explained by the reduced surface oxygen doping effect in DWCNTs as compared to SWCNTs, which is well known to dope the CNT and therefore increases the conductivity [18]. Since surface oxygen adsorption and doping is maximized on SWCNTs because the only CNT shell is completely exposed to air, it's not surprising that SWCNT behaves more metallic than DWCNT. Therefore, the difference in H_2 responsivity measured on the four kinds of Pt-NPs/CNTs/Gr devices in figure 3(a) could be attributed to the compromise of the effective sensor surface area and CNT network conductance. For H_2 sensing, both high surface area and CNT network conductance are desired. With consideration of CNT bundling and the CNT conductance with increasing diameter of the constituent CNTs or CNT bundles in practical CNT films, the best H_2 responsivity on the Pt-NPs/MWCNTs (10 nm)/Gr device can

Nano Express 3 (2022) 035004 M Alamri et al

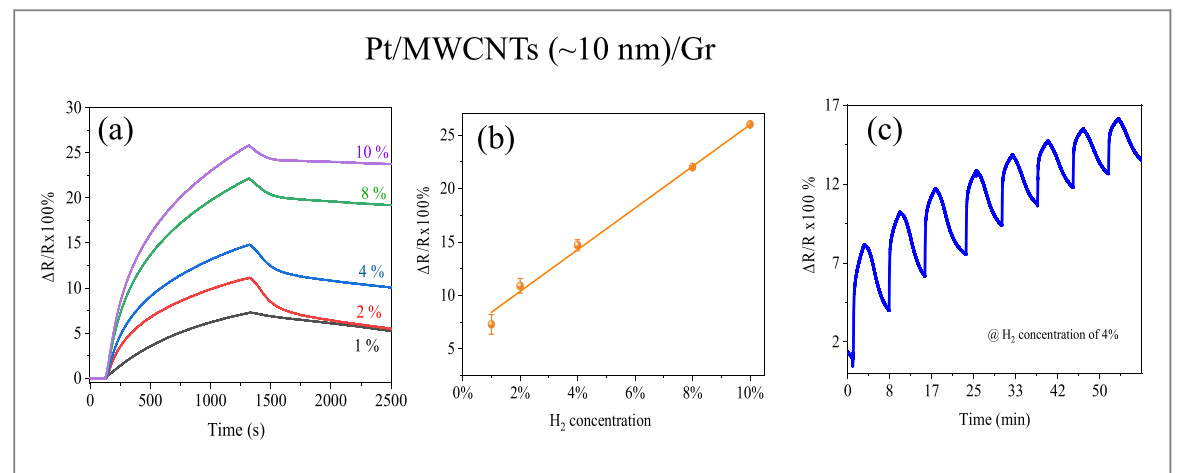


Figure 4. (a) Dynamic response of the Pt-NPs/MWCNTs (\sim 10 nm)/Gr nanohybrids to H₂ of different concentrations in the range from 1% to 10%. (b) H₂ sensitivity as function of H₂ concentration. (c) Dynamic response of Pt-NPs/MWCNTs (\sim 10 nm)/Gr H₂ gas sensor at H₂ concentration of 4%.

be ascribed to the combination of highest effective sensing surface area and conductance in MWCNTs (10 nm) films. Specifically, the SWCNT bundle diameter is comparable to the diameter of the MWCNTs (10 nm). The considerably lower conductance in the latter would lead to better signal transport and hence H₂ sensitivity in the Pt-NPs/MWCNTs (10 nm)/Gr device than its counterpart of SWCNTs. This result also suggests that further improvement of sensor performance is possible by removing the bundling effect in purified metallic SWCNTs films in Pt-NPs/SWCNTs/Gr nanohybrids. Figure 3(c) illustrates the working principle of the Pt-NPs/CNTs/Gr devices. The catalytic Pt-NPs assist dissociation of the H₂ molecules and the follow up transfer of electrons from the Pt-NPs to the CNT and eventually to Gr, which consequently changes the resistance of the Gr channel as H₂ response. The catalytic Pt-NPs assist dissociation of the H₂ molecules, and the resulted H atoms dissolve readily into a Pt layer, lowering its work function. This results in electrons transfer from the Pt layer to the CNT and finally to graphene, thus lowers the resistance of CNT and graphene (which are p-type in ambient)[9, 34].

Figure 4(a) compares the $\rm H_2$ responsivity of the Pt-NPs/MWCNTs (10 nm)/Gr sensors as a function of the $\rm H_2$ concentration. The responsivity decreases linearly when the decreasing $\rm H_2$ concentration is anticipated due to the reduction of the number of the $\rm H_2$ molecules absorbed on the Pt-NPs/MWCNTs/Gr sensors [35]. The approximately linear relationship between the $\rm H_2$ responsivity and $\rm H_2$ concentrations can be observed in figure 4(b). Quantitatively, the responsivity decreases from 26% to 7% when the $\rm H_2$ concentration decreases from 10% to 1%. It should be noted that the concentration of 1% of $\rm H_2$ gas is lower than the threshold of inflammable $\rm H_2$ concentration of 4% [36]. In order to probe the reproducibility, the Pt-NPs/MWCNT/Gr nanohybrid $\rm H_2$ sensor was exposed to repeated cycles of 4% $\rm H_2$ gas pulses and figure 4(c) illustrates the dynamic responses measured. Overall, a good repeatability of the Pt-NPs/MWCNTs/Gr $\rm H_2$ gas sensor has been demonstrated with respect to multiple $\rm H_2$ pulse exposures.

It should be realized that the $\rm H_2$ responsivity of the Pt-NPs/CNTs/Gr nanohybrids can be further enhanced by activating the CNT surface as shown previously on SWCNTs [25]. Figure 5(a) shows the responsivity of the Pt-NPs/MWCNTs (10 nm)/Gr $\rm H_2$ gas sensor to $\rm H_2$ gas at concentrations of 10% (red) and 2% (blue) respectively. The solid curves correspond to the results taken on the as-prepared device while the dashed curves, on the same device after the device was exposed to nondestructive UV irradiation for 5 min. The responsivity of the device increases from 26% (10%) to 36% (20%) for the $\rm H_2$ concentrations of 10% (2%). This result demonstrates that the UV light (360 nm–400 nm) can effectively induce desorption of air molecules from the surface of MWCNTs and graphene [37–41], which improves the $\rm H_2$ sensing performance of the ALD Pt-NPs/MWCNTs (10 nm)/Gr nanohybrid sensors. A similar trend was also observed for the Pt-NPs/SWCNTs/Gr $\rm H_2$ gas sensor to $\rm H_2$ gas at the $\rm H_2$ concentrations of 10% (red, solid and dashed lines) and 2% (blue, solid and dashed lines), as displayed in figure 5(b). Longer time of exposure (> 5 min) to UV light caused a degradation to Gr and CNTs [25].

While most H_2 sensor characterization was carried out in N_2 atmosphere, the practical applications of the H_2 sensors may be in ambient. For ambient operation, a few techniques such as UV illumination, increasing the humidity, and the operating the temperature have shown to improve the recovery time of H_2 gas sensor [42]. In addition, gate-assistant recovery approach has been used for rapid recovery H_2 gas sensors for practical application in ambient [43]. A Al-Diabata *et al* fabricated CNTs-based H_2 gas sensor with a short recovery time and attributed the fast recovery to the large surface to-volume ratio CNTs and the exposure of the device to air for fast recovery [44]. When H_2 detection is performed using air as the carrier gas, H_2 molecules may interact

Nano Express 3 (2022) 035004 M Alamri et al

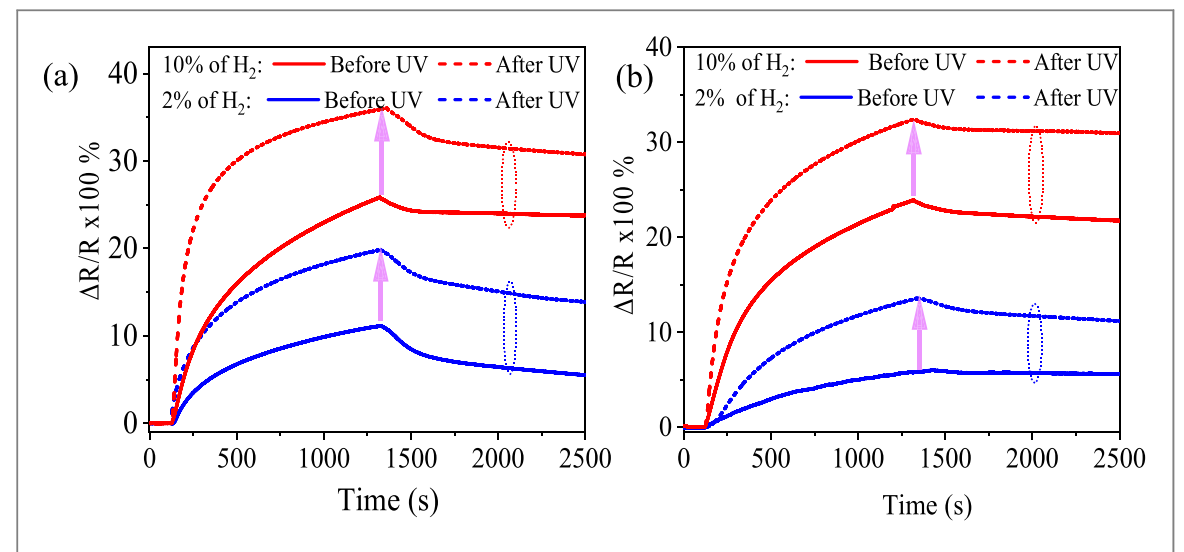
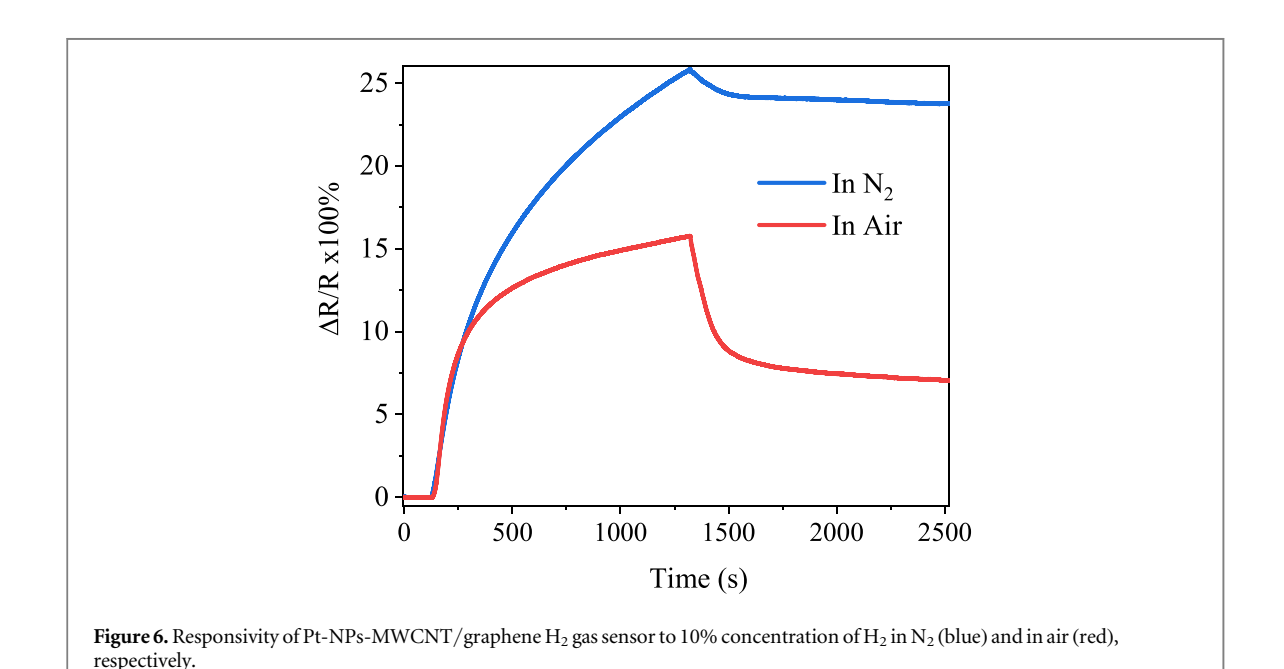


Figure 5. Sensitivity of (a) Pt-NPs/MWCNTs (\sim 10 nm)/Gr H₂ gas sensor before (solid line) and after UV irradiation for 5 min (dashed line) at H₂ concentrations of 10% (red) and 2% (blue), respectively. (b) Pt-NPs/SWCNTs/Gr H₂ gas sensor before (solid line) and after UV irradiation for 5 min (dashed line) at H₂ concentrations of 10% (red) and 2% (blue).



with oxygen in air to produce water molecules [45, 46] and reduces the H_2 molecules adsorbed on the surface of the sensor.

Figure 6 compares the responsivity of the Pt-NPs/MWCNTs (10 nm)/Gr H_2 gas sensor to 10% of H_2 in air (red) and in N_2 (blue) atmosphere. The device indeed exhibits reduced H_2 responsivity in air by about 40%. Interestingly, a considerably faster recovery of the H_2 gas sensor represents the benefit of the in-air detection of H_2 because O_2 molecules in air can facilitate desorption of H_2 molecules from the surface of the Pt-NPs/CNTs/Gr nanohybrids sensors. This result shows that the Pt-NPs/CNTs/Gr nanohybrids sensors are promising for practical applications of H_2 sensing.

Table 1 compares the performance of the Pt-NPs/MWCNT/Gr H_2 gas sensor developed in this work with some representative works of CNT-based gas sensor decorated with Pt. Prior works typically adopted either evaporation or solution based chemical reaction for Pt fabrication, which have disadvantages considering these approaches consume significantly more Pt source during the fabrication while not producing a conformal Pt nanostructure coating on CNTs. In contrast, ALD could efficiently provide a conformal coating of the catalytic Pt-NPs on CNT films as shown in this work. Compared to the SWCNT counterpart, the MWCNT film has the advantage of large surface area and high electrical conductance, both are critical to achieving high sensor

 $\textbf{Table 1.} Comparison of \ H_2 \ sensing \ performance \ with \ early \ reports \ on \ Pt \ decorated \ CNT-based \ H_2 \ sensor. \ Specific \ responsivity \ is \ calculated \ by \ dividing \ H_2 \ responsivity \ by \ the \ H_2 \ concentration.$

Sensor platform	Pt fabrication method	H ₂ concentration	H ₂ responsivity	Specific responsivity	References
superaligned CNT film pulled from forest	evaporation	10%	~7%	0.7	[10]
MWCNT	reaction in solution	4%	6.5%	1.625	[47]
MWCNT	reaction in solution	4%	8%	2	[9]
vertically-aligned CNT	sputtering	1%	1.1%	1.1	[48]
SWCNT/graphene nanohybrid	ALD	10%	7.5%	0.75	[34]
MWCNT/graphene nanohybrid after UV irradiation	ALD	10%	36%	3.6	This Work

responsivity. In addition, UV irradiation helps remove CNT surface to promote H_2 sensing. All these together leads to the much higher H_2 sensitivity up to 36% in our Pt-NPs/MWCNT/Gr H_2 gas sensor.

4. Conclusions

In summary, this work has made a comparative study of the H_2 sensors performance on Pt-NPs/CNTs/Gr nanohybrids with different films of SWCNTs, DWCNTs, MWCNTs (10 nm) and MWCNTs (10–30 nm) of comparable film thicknesses of ~500 nm. In these Pt-NPs/CNTs/Gr sensors, the CNT film determines the effective sensing area and the signal transport to Gr channel. With increasing diameter of the CNTs from ~1 nm for SWCNTs, to ~2 nm for DWCNTs, and 10 nm and up to 30 nm respectively for two kinds of MWCNTs, the constituent CNT aspect ratio (since the CNT lengths are fixed in the range of 5–10 μ m) and the effective sensing area can be systematically varied. On the other hand, CNT conductivity can be also varied systematically considering the CNT bandgap is proportional inversely to the CNT diameter, leading to more metallic CNTs at larger CNT diameters. This study has revealed that the performance of the Pt-NPs/CNTs/Gr H_2 sensors is the compromise of the effective sensing area and electric conductivity. Among different CNT assessed, the best performance was observed on Pt-NPs/CNTs/Gr H_2 sensors with a MWCNT film of CNT diameter of ~10 nm. The highest response is about 26% when Pt-NPs/MWCNTs/Gr to H_2 concentration of 10% before UV radiation. In comparison with its counterparts using SWCNTs and DWCNTs that surfer CNT bundling, this MWCNTs film has a comparable sensing area but considerably better electrical conductance, revealing the critical importance of the high electric conductivity in the MWCNTs for an efficient charge transfer.

Acknowledgments

This research was supported by Plant Directed Research and Development funds from the Department of Energy's Kansas City National Security Campus, operated and managed by Honeywell Federal Manufacturing and Technologies, LLC. under contract. No. DE-NA-0002839 with the U.S. Department of Energy/National Nuclear Security Administration. The authors also acknowledge support in part by NSF contracts Nos. NSF-DMR-1909292, and NSF-ECCS-1809293. M A acknowledges the support from Umm Al-Qura University.

Data availability statement

All data that support the findings of this study are included within the article (and any supplementary files).

Supplementary material

See Supplementary Material for optical images and Raman maps of graphene and MWCNT/graphene. Also, EDS spectra of 50 C ALD-Pt @ SWCNT film, DWCNT film, and MWCNT films are included in the Supplementary Material.

ORCID iDs

Mohammed Alamri https://orcid.org/0000-0002-7473-8644 Judy Z Wu https://orcid.org/0000-0001-7040-4420

References

- [1] Sinha N, Ma J and Yeow J T 2006 Carbon nanotube-based sensors J. Nanosci. Nanotechnol. 6 573–90
- [2] Zhang T, Mubeen S, Myung N V and Deshusses M A 2008 Recent progress in carbon nanotube-based gas sensors *Nanotechnology* 19 332001
- [3] Sutthinet C, Sangnual A and Phetchakul T 2009 Alcohol sensor based on multi-wall carbon nanotube *Proc. of the 2009 12th Int. Symp. on Integrated Circuits, IEEE* pp. 321–3
- [4] Giordano C, Filatrella G, Sarno M and Di A 2019 Bartolomeo, Multi-walled carbon nanotube films for the measurement of the alcoholic concentration *Micro & Nano Letters* 14 304–8
- [5] Zhao J, Buldum A, Han J and Lu J P 2002 Gas molecule adsorption in carbon nanotubes and nanotube bundles *Nanotechnology* 13 195–200
- [6] Mubeen S, Zhang T, Yoo B, Deshusses M A and Myung N V 2007 Palladium nanoparticles decorated single-walled carbon nanotube hydrogen sensor *J. Phys. Chem. C Nanomater. Interfaces* 111 6321–7
- [7] Zilli D, Bonelli PR and Cukierman A L 2011 Room temperature hydrogen gas sensor nanocomposite based on Pd-decorated multiwalled carbon nanotubes thin films Sens. Actuators B Chem. 157 169–76

M Alamri et al

- [8] Braun E I, Huang A, Tusa C A, Yukica M A and Pantano P 2016 Use of Raman spectroscopy to identify carbon nanotube contamination at an analytical balance workstation *Journal of occupational and environmental hygiene* 13 915–23
- [9] Kaniyoor A and Ramaprabhu S 2011 Hybrid carbon nanostructured ensembles as chemiresistive hydrogen gas sensors Carbon 49 227–36
- [10] Jung D, Han M and Lee G S 2015 Fast-response room temperature hydrogen gas sensors using platinum-coated spin-capable carbon nanotubes ACS Appl. Mater. Interfaces 7 3050–7
- [11] Kaniyoor A, Jafri R I, Arockiadoss T and Ramaprabhu S 2009 Nanostructured Pt decorated graphene and multi walled carbon nanotube based room temperature hydrogen gas sensor Nanoscale 1 382-6
- [12] Liu B, Alamri M, Walsh M, Doolin J L, Berrie C L and Wu J Z 2020 Development of an ALD-Pt@SWCNT/graphene 3D nanohybrid architecture for hydrogen sensing ACS Appl. Mater. Interfaces 12 53115
- [13] Geim A K 2009 Graphene: status and prospects Science 324 1530-4
- [14] Chen J-H, Jang C, Xiao S, Ishigami M and Fuhrer M S 2008 Intrinsic and extrinsic performance limits of graphene devices on SiO₂ Nat. Nanotechnol. 3 206–9
- [15] Gahoi A, Passi V, Kataria S, Wagner S, Bablich A and Lemme M C 2015 Systematic comparison of metal contacts on CVD graphene 2015 45th European Solid State Device Research Conf. (ESSDERC) pp 184–7
- [16] Gong M, Liu Q, Cook B, Kattel B, Wang T, Chan W L, Ewing D, Casper M, Stramel A and Wu J Z 2017 All-printable ZnO quantum dots/Graphene van der Waals heterostructures for ultrasensitive detection of Ultraviolet light ACS Nano 11 4114–23
- [17] Xu G, Lu R, Liu J, Chiu H-Y, Hui R and Wu J Z 2014 Photodetection based on ionic liquid gated plasmonic Ag nanoparticle/graphene nanohybrid field effect transistors Adv. Opt. Mater. 2729–36
- [18] Lu R, Xu G and Wu J Z 2008 Effects of thermal annealing on noise property and temperature coefficient of resistance of single-walled carbon nanotube films *Appl. Phys. Lett.* 93 213101
- [19] Rakitin A, Papadopoulos C and Xu J 2000 Electronic properties of amorphous carbon nanotubes Physical Review B 61 5793
- [20] Zhang F, Hou P-X, Liu C, Wang B-W, Jiang H, Chen M-L, Sun D-M, Li J-C, Cong H-T and Kauppinen E I 2016 Growth of semiconducting single-wall carbon nanotubes with a narrow band-gap distribution *Nat. Commun.* 7 1–9
- [21] Alamri M, Liu B, Sadeghi S M, Ewing D, Wilson A, Doolin J L, Berrie C L and Wu J 2020 Graphene/WS₂ Nanodisk Van der waals heterostructures on plasmonic ag nanoparticle-embedded silica metafilms for high-performance photodetectors ACS Appl. Nano Mater. 3 7858–68
- [22] Liu Q, Gong Y, Wilt J S, Sakidja R and Wu J 2015 Synchronous growth of AB-stacked bilayer graphene on Cu by simply controlling hydrogen pressure in CVD process *Carbon* 93 199–206
- [23] Wu Z, Chen Z, Du X, Logan J M, Sippel J, Nikolou M, Kamaras K, Reynolds J R, Tanner D B and Hebard A F 2004 Transparent, conductive carbon nanotube films *Science* 305 1273–6
- [24] Lu R, Li Z, Xu G and Wu J Z 2009 Suspending single-wall carbon nanotube thin film infrared bolometers on microchannels Appl. Phys. Lett. 94 163110
- [25] Alamri M A, Liu B, Walsh M, Doolin J L, Berrie C L and Wu J Z 2021 Enhanced H₂ sensitivity in ultraviolet-activated Pt nanoparticle/ SWCNT/graphene nanohybrids IEEE Sens. J. 21 19762–70
- [26] Ferrari A C, Meyer J, Scardaci V, Casiraghi C, Lazzeri M, Mauri F, Piscanec S, Jiang D, Novoselov K and Roth S 2006 Raman spectrum of graphene and graphene layers *Phys. Rev. Lett.* **97** 187401
- [27] Pyo S, Choi J, Kim J and Fully A 2019 Transparent, flexible, sensitive, and visible-blind ultraviolet sensor based on carbon nanotube—graphene hybrid Adv. Electron. Mater. 5 1800737
- [28] Piscanec S, Lazzeri M, Robertson J, Ferrari A C and Mauri F 2007 Optical phonons in carbon nanotubes: Kohn anomalies, Peierls distortions, and dynamic effects *Physical Review B* 75 035427
- [29] Brown S, Jorio A, Dresselhaus M and Dresselhaus G 2001 Observations of the D-band feature in the Raman spectra of carbon nanotubes *Physical Review B* 64 073403
- [30] Deng L, Young R J, Kinloch I A, Sun R, Zhang G, Noé L and Monthioux M 2014 Coefficient of thermal expansion of carbon nanotubes measured by Raman spectroscopy *Appl. Phys. Lett.* **104** 051907
- [31] Duesberg G, Loa I, Burghard M, Syassen K and Roth S 2000 Polarized Raman spectroscopy on isolated single-wall carbon nanotubes Phys. Rev. Lett. 85 5436
- [32] Costa S, Borowiak-Palen E, Kruszynska M, Bachmatiuk A and Kalenczuk R 2008 Characterization of carbon nanotubes by Raman spectroscopy Materials Science-Poland 26 433—41
- [33] Chen R J, Franklin N R, Kong J, Cao J, Tombler T W, Zhang Y and Dai H 2001 Molecular photodesorption from single-walled carbon nanotubes Appl. Phys. Lett. 79 2258–60
- [34] Liu B, Alamri M, Walsh M, Doolin J L, Berrie C L and Wu J Z 2020 Development of an ALD-Pt@SWCNT/Graphene 3D nanohybrid architecture for hydrogen sensing ACS Appl. Mater. Interfaces 12 53115–24
- [35] Hao L, Liu Y, Du Y, Chen Z, Han Z, Xu Z and Zhu J 2017 Highly enhanced H₂ sensing performance of few-layer MoS₂/SiO₂/Si heterojunctions by surface decoration of Pd nanoparticles *Nanoscale Res. Lett.* 12 567
- [36] Sayago I, Terrado E, Lafuente E, Horrillo M, Maser W K, Benito A, Navarro R, Urriolabeitia E, Martinez M and Gutierrez J 2005 Hydrogen sensors based on carbon nanotubes thin films Synth. Met. 148 15–9
- [37] Yang L, Ouyang M, Li W J and Han X 2008 UV-illumination induced desorption of CNT sensors 2008 8th IEEE Conf. on Nanotechnology, IEEE pp. 284–7
- [38] Kang C G, Lee S K, Choe S, Lee Y G, Lee C-L and Lee B H 2013 Intrinsic photocurrent characteristics of graphene photodetectors passivated with Al₂O₃ Opt. Express 21 23391–400
- [39] Muckley E S, Nelson A J, Jacobs C B and Ivanov I N 2016 Multimodal probing of oxygen and water interaction with metallic and semiconducting carbon nanotube networks under ultraviolet irradiation *Journal of Photonics for Energy* 6 025506
- [40] Chen G, Paronyan T M, Pigos E M and Harutyunyan A R 2012 Enhanced gas sensing in pristine carbon nanotubes under continuous ultraviolet light illumination Sci. Rep. 2 1–7
- [41] Kim S J, Han J-W, Kim B and Meyyappan M 2017 Single walled carbon nanotube based air pocket encapsulated ultraviolet sensor ACS Sens. 2 1679–83
- [42] Hashtroudi H, Yu A, Juodkazis S and Shafiei M 2022 Ultra-sensitive photo-induced hydrogen gas sensor based on two-dimensional CeO₂-Pd-PDA/rGO heterojunction nanocomposite *Nanomaterials* 12 1628
- [43] Liu F, Xiao M, Ning Y, Zhou S, He J, Lin Y and Zhang Z 2022 Toward practical gas sensing with rapid recovery semiconducting carbon nanotube film sensors *Science China Information Sciences* 65 1–8
- [44] Al-Diabat A M, Algadri N A, Ahmed N M, Abuelsamen A and Bidier S A 2021 A high-sensitivity hydrogen gas sensor based on carbon nanotubes fabricated on SiO₂ substrate *Nanocomposites* 7 172–83

Nano Express 3 (2022) 035004 M Alamri et al

[45] Gagaoudakis E, Panagiotopoulos A, Maksudov T, Moschogiannaki M, Katerinopoulou D, Kakavelakis G, Kiriakidis G, Binas V, Kymakis E and Petridis K 2020 Self-powered, flexible and room temperature operated solution processed hybrid metal halide p-type sensing element for efficient hydrogen detection J. Phys.: Mater. 3 014010

- [46] Gupta D, Dutta D, Kumar M, Barman P, Sarkar C, Basu S and Hazra S 2014 A low temperature hydrogen sensor based on palladium nanoparticles Sensors Actuators B 196 215–22
- [47] Kumar M K and Ramaprabhu S 2006 Nanostructured Pt functionlized multiwalled carbon nanotube based hydrogen sensor J. Phys. Chem. B 110 11291-8
- [48] Penza M, Rossi R, Alvisi M, Signore M A, Cassano G, Dimaio D, Pentassuglia R, Piscopiello E, Serra E and Falconieri M 2009 Characterization of metal-modified and vertically-aligned carbon nanotube films for functionally enhanced gas sensor applications Thin Solid Films 517 6211–6